AIAA JOURNAL
Vol. 36, No. 7, July 1998

Velocity and Density Measurements in Supersonic High-Temperature Exhaust Plumes

L. Y. Jiang* and J. P. Sislian†
University of Toronto, Downsview, Ontario M3H 5T6, Canada

A two-dimensional laser Doppler velocimeter and a Rayleigh scattering system were used to measure the mean velocities, turbulence quantities, and mean density in a supersonic high-temperature exhaust plume with and without an annular base flow. The distributions of mean temperature and Mach number were inferred. For both cases, the potential core of the supersonic jet extends about 6 nozzle diameters, and the flow remains supersonic until about 15 nozzle diameters. The mean axial velocity, turbulence kinetic energy, shear stress, and temperature become self-similar downstream of the flow. Similarities of turbulence quantities develop slower than the mean velocity, whereas the temperature similarity is established upstream of the velocity. Near the nozzle base of the coaxial jets, one and a half recirculation zones are formed, which represents an extreme of the central-jet-dominated coaxial flows.

Introduction

SUPERSONIC jet mixing is closely related to a number of engineering applications. With the development of laser diagnostics, many experimental studies on supersonic jet mixing have been carried out. In an attempt to understand the noise-generating mechanism, researchers such as Lau et al.[1] and Lau[2] measured mean and fluctuating velocities in supersonic free jets. They found that the jet growth rate decreases with Mach number and the potential core contracts with jet-exit temperature. Because of developments in hypersonic propulsion, a significant number of experiments on the compressible planar mixing layers have been performed over the last 10 years. Dimotakis[3] reviewed these studies and pointed out that the shear-layer growth decreases with increasing convective Mach number and with increasing density and velocity ratios of both streams. To study the exhaust flow patterns of flying vehicles, Petrie and Walker[4] made laser Doppler velocimeter (LDV) measurements of the mean velocity components and turbulence kinetic energy in coflowing air/air plumes. In their experiment, a large bluff base configuration was used, and typical shock wave structures were investigated.

In contrast to velocity measurements, density and temperature measurements in supersonic flows are rare. Using a spontaneous Raman scattering technique, de Groot and Weiss[5] reported temperature and species measurements at one cross section in the plume of a 110-N gaseous hydrogen/oxygen thruster. Recently, Cheng et al.,[6] using a Raman scattering and laser-induced predissociative fluorescence technique, measured the mean and fluctuating quantities of temperature, major species, and OH radical concentration in a supersonic lifted coflowing hydrogen–air flame.

A literature survey shows that detailed velocity and density measurements in supersonic flows are lacking, especially for missile-type configurations. Presented here are the velocity and density measurements of a supersonic high-temperature exhaust plume with and without an annular base flow. The plume has a Mach number of 1.8 and a total temperature of ~1600 K. The objective of this study is to shed some light on the turbulent mixing of supersonic high-temperature exhaust plumes and to provide a database for numerical modeling. Typical shock wave structures and afterburning phenomena in rocket plumes are not included in this phase of the study.

Received Feb. 10, 1997; revision received Feb. 27, 1998; accepted for publication March 13, 1998.

*Research Assistant, Institute for Aerospace Studies; currently Associate Research Officer, Aerodynamics Laboratory, Institute for Aerospace Research, National Research Council, Ottawa, Ontario K1A 0R6, Canada.

†Professor, Institute for Aerospace Studies, 4925 Dufferin Street. Associate Fellow AIAA.

Experimental Setup

A test rig for generating a supersonic high-temperature jet was designed and fabricated. The nozzle exit geometry of the test rig is schematically shown in Fig. 1. The supersonic nozzle made of molybdenum has an exit diameter of 8 mm, and its contour is designed for shock-free flow at the exit. The outer diameter of the annular nozzle is 50.8 mm, and the width of the annular channel is 7 mm. Compressed air and gas were properly filtered, regulated, and metered. Natural gas mixed with air was burned at a pressure of 5.6 bar in a water-cooled combustion chamber and ejected from the central nozzle. The annular air passed two perforated plates and was ejected from the annular nozzle at 100 m/s. For velocity measurements, the fuel/air equivalence ratio was 0.94, and the Al_2O_3 aerosol with a nominal size of 0.05 μm was introduced from two seeding generators into the central and annular flows.

The test rig provided safe, stable, and durable operations. Variation of the jet exit flow parameters was less than 2% during 5 h of continuous testing. The test rig was mounted on a three-dimensional, computer-controlled rigid traverse system, and an indication system with 0.01-mm resolution was used to measure the rig position. To minimize room disturbances, the test rig was placed within a screen enclosure having dimensions 1.5 × 1.2 × 2.7 m high. More details of the test facilities are given in Refs. 7 and 8.

LDV

The two-dimensional LDV was operated in off-axis forward scatter mode. A Spectra Physics Model 171-17 argon laser was used as the light source with 4-W output. The optical system was built up from standard Dantec 55x modular optic components, and two Thermal Systems Incorporated 1990 counters were used to process signals from photomultipliers.

LDV measurements in high-velocity turbulent flows pose some difficult problems. Few researchers have performed velocity measurements over 1000 m/s (Refs. 9 and 10). The high velocity leads to high Doppler frequency. Unfortunately, the maximum acceptable frequency of the present signal processors is limited to ~100 MHz (Ref. 10). Consequently, the probe volume size reduction is restricted. On the other hand, the steep velocity gradients in supersonic mixing layers require a small probe volume to reduce velocity gradient bias, and submicrometer seeding particles used in the experiments prefer a small probe volume to increase light scattering and signal-to-noise ratio. Moreover, to resolve all length scales in turbulent flows, a small probe volume is also required.

A comprehensive optimization of the LDV system was performed, and different LDV configurations were analyzed and tested (details are given in Ref. 8). For most of the velocity measurements, the control volume diameter was 0.13 mm with a length of 0.6 mm. For the measurement of mean radial velocity in the vicinity of the potential core region, the laser beam expander was removed to

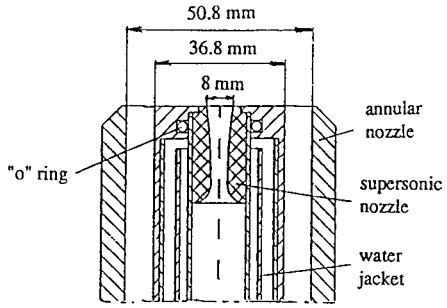

Fig. 1 Close-up view of the nozzles.

reduce fringe bias and counter digitization error. As a result, the control volume diameter was doubled. Because the mean radial velocity gradient was small in this study, the introduced velocity gradient bias on the mean radial velocity was negligible. To minimize velocity gradient bias, the length of the control volume was kept tangential to the axially symmetric mean velocity contours. Because the velocity gradient in the flow tangential direction was zero, the velocity variation along the axis of the control volume was greatly reduced.

Other bias errors and statistical errors related to LDV measurements, such as the effect of large seeding particles, counterdigitization error, velocity bias, frequency response bias of counters, and nonuniform seeding bias, were also analyzed and controlled. Usually two sets of 10,000 samples for each were taken at each measurement point. The statistical errors of mean velocity components, turbulent fluctuating velocities, and shear stress were calculated[7] for each measurement. Considering other errors, the overall measurement errors are estimated as follows: mean axial velocity $U \sim 2\%$, mean radial velocity $V \sim 10\%$, shear stress $uv \sim 7\%$, and u, v, and w rms of fluctuating velocities $\sim 5\%$.

Rayleigh Scattering Measurement

Rayleigh Scattering

For a Rayleigh scattering system, the signal intensity from Rayleigh scattering at a spatial position in the flow is dependent on the total molecular number density and Rayleigh scattering cross section of the mixture.[11] That is,

$$I = CN \sum \left(\frac{\partial \sigma}{\partial \Omega} \right)_i X_i \tag{1}$$

where I is the signal intensity from Rayleigh scattering, N is the total number density, $(\partial\sigma/\partial\Omega)_i$ and X_i are the Rayleigh cross section and the mole fraction of the ith species, respectively, and C is a constant dependent on a specific Rayleigh scattering system.

To isolate the dependence of the scattered light intensity to just the total number density, it is necessary to keep the Rayleigh scattering cross section of the combustion products equal to that of air. During Rayleigh scattering measurements, 7% helium in volume of the central flow rate was added into the central air, and the fuel/air equivalence ratio was raised to unity to maintain the same temperature as that for velocity measurements. The Rayleigh scattering cross sections of the involved species for laser excitation at 514.5 nm were given by Long.[12] The difference of Rayleigh scattering cross section between the exhaust mixture and air was 0.3%, whereas for the LDV case the discrepancy was 7.2%. The ratios of specific heat and viscosity of exhaust mixtures between the density and velocity measurements were 0.96 and 1.00, respectively. The effects of operating condition on temperature and velocity flowfield were within the measurement accuracy.

There is some ambiguity about the interpretation of Rayleigh scattering intensity as temperature in turbulent flows. The physical meaning of inferred temperature from the number density measurement in turbulent flows can be clarified by introducing the molecular number density weighted temperature. By analogy to the Favre mass density average, a number density weighted mean temperature $\tilde{T}$ and the corresponding fluctuating temperature T'' can be defined:

$$\tilde{T} \equiv \overline{NT}/\bar{N} \tag{2}$$

and

$$T = \tilde{T} + T'' \tag{3}$$

where T and N are the instantaneous temperature and number density of the gas mixture. Then the time-averaged gas state equation can be expressed as

$$\bar{P} = k(\bar{N}\tilde{T} + \overline{NT}'') = k\bar{N}\tilde{T} \tag{4}$$

where k ($1.38054\,10^{-23}$ J/K) is Boltzmann's constant and $\overline{NT}'' = 0$. Averaging Eq. (1) over time and substituting Eq. (4) into it, we can obtain the number density weighted mean temperature

$$\tilde{T} = C\frac{\bar{P}}{k\bar{I}} \sum \left(\frac{\partial \sigma}{\partial \Omega_i} \right) X_i \tag{5}$$

Note that the turbulent transfer of all species is assumed to be identical, i.e., the Rayleigh scattering cross section $\sum(\partial\sigma/\partial\Omega)_i X_i$ is constant over time at each spatial position in the flow.

Given temperature and velocity distributions in the flowfield, the distribution of Mach number can be determined:

$$M = \frac{|\boldsymbol{U}|}{\sqrt{\gamma_{\text{loc}} R\tilde{T}/W_{\text{loc}}}} \tag{6}$$

where γ_{loc} is the local specific heat ratio, W_{loc} is the local molecular weight, and R is the universal gas constant. With the assumption that the thermal flowfield is similar to the chemical species flowfield (Lewis number = 1), the local molecular weight and specific heat ratio are linearly interpolated based on the measured mean temperature. Because the differences of specific heat ratio and molecular weight between the exhaust mixture and air are less than 3%, the introduced uncertainty is negligible.

Rayleigh System and Density Measurement

A Rayleigh scattering system similar to that used by Dibble and Hollenbach[13] was developed. The Spectra Physics Model 171-17 argon laser gave 2 W of power at the wavelength 514.5 nm, and the laser diameter was 0.13 mm at the waist. A pair of plano-convex lenses with $f = 254$ mm and $d = 101.6$ mm ($f\# = 2.5$) was used to collect the scattered laser light at 90 deg to the laser axis and its plane of polarization. The collected light was focused onto a 0.6-mm-diam pinhole, which made the measuring volume of the Rayleigh scattering system the same as that of the LDV measurement. After the pinhole, the light passed through a polarizer and an interference filter and then reached a Hamamatsu Model R647-04 photomultiplier. The photoelectron pulses from the photomultiplier were amplified and counted by a Stanford Research Systems SR400 photon counter. The maximum counting rate was 200 MHz with a time resolution of 1 ns. With this setup, the Rayleigh scattering signal was $\sim 3 \times 10^6$ counts/s for air at room temperature of $\sim$293 K. The entire transmission and collection optics were covered by black shields. All windows were covered with black cloth, and all room lights, except for two red lamps, were turned off during the density measurements. The background noise was surveyed over the flowfield by offsetting the measurement volume of the collection optics 2 mm above the laser beam. The noise from the background and dark count was less than 0.5% of the signal level for $Z/d \geq 1$. No measurement was made at the initial section $Z/d = 0.25$ due to the laser reflection from the nozzle exit surface.

For the single jet, a very-low-velocity, filtered, coflowing airstream was employed. The coflowing air had a large diameter of 80 mm, and its velocity was 0.4% of the central jet velocity. With this arrangement, the effect of particles from the environment on the Rayleigh signal was eliminated at upstream sections. The gate of the photon counter was set to 0.5 s, and two samples were taken for each spatial position. The total pulses recorded in two samples ranged from 3×10^6 to 0.8×10^6. For the density measurements at downstream sections, $Z/d \geq 10$, particles from the surrounding air could enter the mixing layer due to turbulent mixing between the jets and surrounding air. Because the Mie scattering (particle scattering) was intermittent in the signal and its photoelectron pulse rate was excessively higher compared with the photoelectron rate produced by Rayleigh scattering, there was no difficulty to reject Mie scattering in the data processing. A 10-μs gate period was selected, and 4000 samples were taken for each spatial point in the

flow. The averaged total pulses from Rayleigh scattering in 4000 samples varied from $\sim 1.2 \times 10^5$ to $\sim 4 \times 10^4$. Samples from particle scattering were rejected according to the 3σ (three times the standard deviation) criterion,[14] and rejected samples were about 2%.

The scattering and detection of photons is a random process, and photoelectron arrival can be modeled by Poisson statistics.[11] Based on the preceding operating parameters, the estimated maximum shot noise error was less than 0.5%, and the maximum pulse pile-up error was 1.8%.

Results and Discussion

Flow Visualization

The flowfields of both single and coaxial jets are visualized by schlieren and laser light sheet techniques. Figure 2 is a schlieren photograph of the coaxial jets. In the upstream region, a recirculation region is formed above the bluff-body surface and extends about 2.5 jet diameters downstream. The smooth region of the inner boundary, between the central jet and the recirculation region, is about two diameters long. Downstream of this region, the boundary of the jet becomes jagged, and vortices are observed in the mixing layer. The size of vortices increases with axial distance, and vortices propagate outward. The annular flow, which is entrained by the central jet, is forced to bend toward the central jet and impinges on it at approximately three to five diameters downstream. The flowfield is surrounded by Mach waves from the end of the recirculation region to about 18 diameters downstream.

Mean Density and Temperature

The mean molecular number density and inferred number-density weighted temperature were obtained at 13 cross sections, $Z/d =$ 1, 2, 3.5, 5, 7.5, 10, 12.5, 15, 17.5, 20, 30, 40, and 50, and along the central axis for both the single and coaxial jets. Shown in Fig. 3 are the mean density and temperature distributions along the central axis from the exit up to $Z/d = 15$. The number density is normalized by the density of air at 293 K. For the single jet, the density and temperature remain nearly constant up to about six diameters downstream; for the coaxial jets, the potential core is slightly shorter than six diameters. In the potential cores of both flows, the normalized molecular number density is about 0.27, and the temperature is about 1080 K. Beyond the potential core, the temperature of the coaxial jets is lower than that of the single jet with a maximum difference of 82 K at $Z/d = 10$. Downstream of this section, the differences of density and temperature between the two flows become smaller.

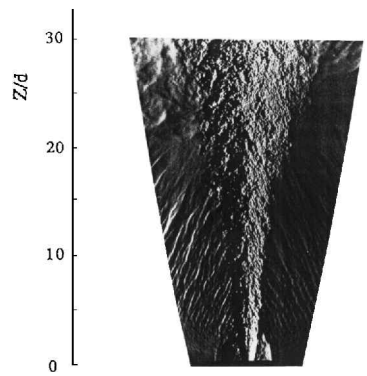

Fig. 2 Schlieren photograph of the coaxial jets.

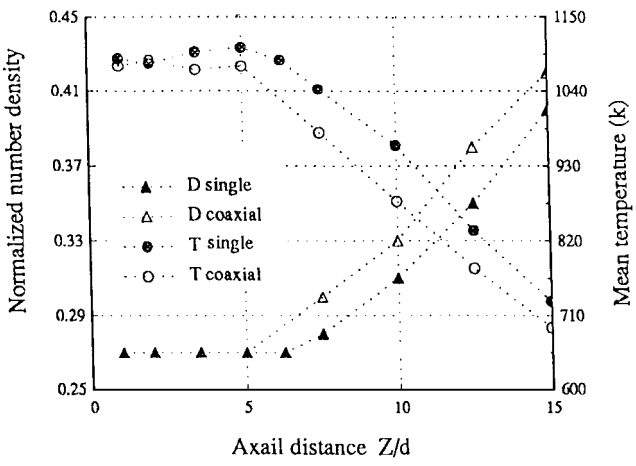

Fig. 3 Density D and temperature T profiles along the center axis.

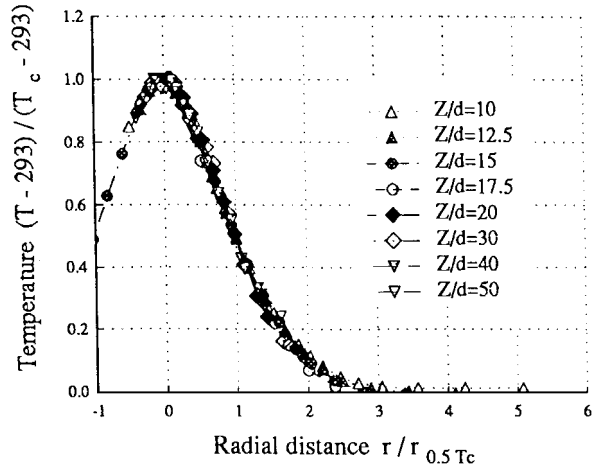

Fig. 4 Similarity of temperature profiles for the single jet.

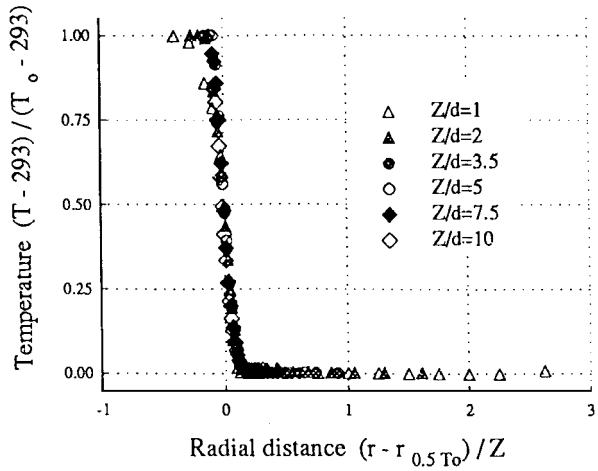

Fig. 5 Normalized temperature profiles for the single jet.

The radial profiles of mean temperature distributions are similar for both flows. Figure 4 shows the similarity of the radial distributions of mean temperature from section $Z/d = 10$–50 for the single jet. The temperature profiles for these downstream sections are normalized in $(T - 293)/(T_c - 293)$ and $r/r_{0.5T_c}$ coordinates, where T_c is the centerline temperature and $r_{0.5T_c}$ is the radial distance with the excess temperature $(T - 293)$ equal to one-half of the center excess temperature $(T_c - 293)$. In Fig. 4, the profiles of $Z/d = 10$–50 collapse onto a single curve. Von Glahn[15] has shown that this normalization of temperature can be applied even to the upstream section $Z/d = 8$ for low-Mach-number jet plumes ($M =$ 0.08–0.7). This self-preservation or local invariance indicates that the flow is fully developed and mainly determined by local parameters such as time and length scales. In other words, the flow is in some state of dynamical equilibrium, and past events do not dominate the dynamics. Figure 5 shows the normalized temperature profiles for the single jet at upstream sections $Z/d =$ 1–10. For these upstream sections, the radial distributions of mean temperature are normalized in $(T - 293)/(T_0 - 293)$ and $(r - r_{0.5T_0})/Z$ coordinates, where T_0 is the jet exit temperature and $r_{0.5T_0}$ is the radial distance with the excess temperature equal to one-half of the jet exit excess temperature $(T_0 - 293)$. All profiles can be described by a single curve. Although this normalization was developed only for core flows, this parametric normalization method can be extended to sections above the potential core. This has also been shown by Lau et al.[1] and Lau.[2]

Similar results are obtained for the coaxial jets. The radial mean temperature profiles of the coaxial jets at eight downstream

cross sections ($Z/d = 10$–50) can be represented by a single curve. In the upstream region of the coaxial jets ($Z/d = 1$–10), the experimental results at sections $Z/d = 1$ and 2 deviate from the normalized curve as expected. The normalization developed by Gortler in 1942[15] is for jets and shear flows and is not suitable for coaxial flows. However, because the velocity ratio of the annular jet to the central jet is only $\frac{1}{12}$, the recirculation region is not strongly developed, and its effect on the temperature flowfield is limited. Therefore, this normalization method can apply for $Z/d > 3.5$ (outside the recirculation region).

Mean and Fluctuating Velocities and Mach Number

The mean velocity components U and V, fluctuating velocities $\sqrt{\bar{u}'^2}$, $\sqrt{\bar{v}'^2}$, and $\sqrt{\bar{w}'^2}$, turbulence kinetic energy $k = (\bar{u}'^2 + \bar{v}'^2 + \bar{w}'^2)/2$, shear stress $\overline{u'v'}$, and relative turbulence intensity $s = \sqrt{k}/\sqrt{(U^2 + V^2)}$ were obtained at 10 cross sections, $Z/d = 0.25$, 2, 5, 7.5, 10, 15, 20, 30, 40, and 50, and along the axis for both the single and coaxial jets. The recirculation region in the coaxial jet flow was mapped in detail. Mach number distributions were calculated at sections $Z/d = 2$, 5, 7.5, 10, 15, 20, 30, 40, and 50 and along the central axis.

Figures 6 illustrates the comparisons of mean axial velocity and Mach number along the central axis between the single and coaxial flows for $Z/d = 0.25$–15. The potential core extends about six diameters downstream for both flows. In the potential core, the mean axial velocity is ~1170 m/s, and the corresponding Mach number is 1.8. Beyond the potential core, the mean axial velocity and Mach number decrease for both flows; however, the decay is faster for the coaxial jets at upstream locations. The maximum difference of mean axial velocity between the two flows is 90 m/s, and the maximum difference of Mach number is 0.08. These maximum differences occur at location $Z/d = 10$, where the temperature difference also reaches a maximum as mentioned earlier. Both flows become subsonic for downstream positions greater than $Z/d \simeq 14.5$.

Figure 7 shows the comparison of fluctuating velocities along the central axis between the single and coaxial flows for $Z/d = 0.25$–15. In the potential core, all turbulence quantities for both flows are relatively small but rapidly increase afterward. The maximum axial fluctuating velocity in the coaxial jets is 198 m/s at $Z/d = 8.75$, whereas the maximum axial fluctuating velocity in the single jet is 165 m/s at $Z/d = 11.25$. The location of the maximum axial fluctuating velocity in the single jet is shifted 2.5 diameters downstream. Large differences of the axial fluctuating velocity between two flows occur in the region $Z/d = 7.5$–10.

The flow structure defines the flow behavior. Because of the presence of the bluff body (or base), the turbulent mixing is much enhanced by the recirculation (or flow separation) and impingement (or reattachment) between the central and annular jets. From the schlieren photo, the impingement occurs in the range of $Z/d = 3$–5 between the annual jet and the central jet. The enhanced turbulence is propagated downstream and toward the central axis. This may explain the preceding observations: The turbulent quantities in the coaxial jets are much higher than those in the single jet in the region

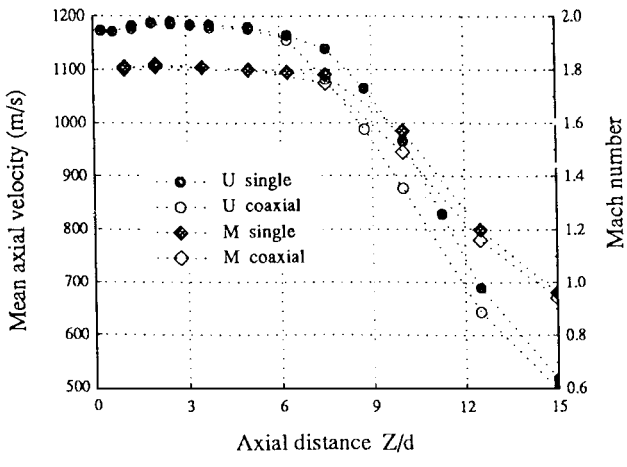

Fig. 6 Mean axial velocity and *M* number along the center axis.

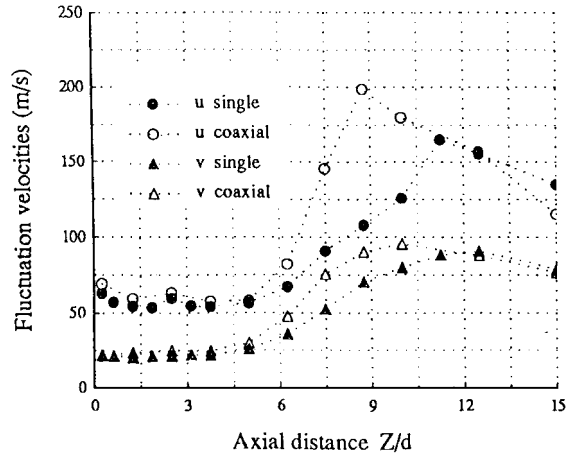

Fig. 7 Fluctuating velocities along the center axis.

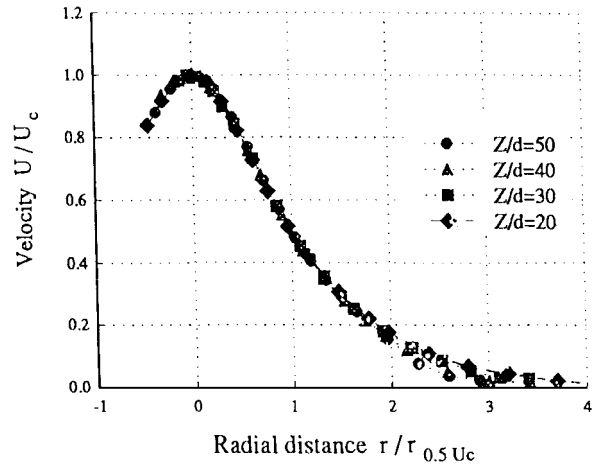

Fig. 8 Similarity of mean axial velocity profiles for the coaxial jets.

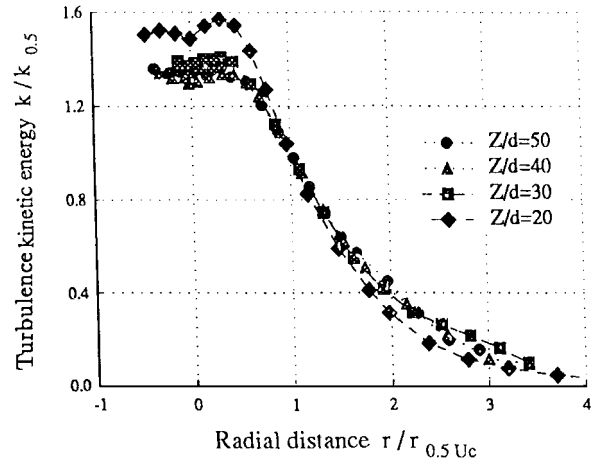

Fig. 9 Similarity of turbulence kinetic energy for the coaxial jets.

$Z/d = 7.5$–10, and large differences of mean temperature, mean axial velocity, and Mach number between two flows appear in this region. With the gradual attenuation of this turbulence enhancement in the coaxial jets, these differences become smaller for Z/d greater than 10.

Similar to the temperature distributions, the velocity profiles can also be expressed in self-similar form. The normalized mean axial velocity, shear stress, and turbulence kinetic energy of the coaxial jets at four downstream cross sections are shown in Figs. 8, 9, and 10 with the coordinates U/U_c, $k/k_{0.5}$, $\overline{u'v'}/(\overline{u'v'})_{0.5}$, and $r/r_{0.5U_c}$, respectively. Figure 8 indicates that the radial profiles of mean axial velocities at sections $Z/d = 20$–50 can be described by a single

Table 1 Turbulent scales of the supersonic exhaust plume

Z/d	r/d	U, m/s	$\sqrt{(\bar{u}'^2+\bar{v}'^2+\bar{w}'^2)}$, m/s	T, K	$\nu \times 10^6$, m^2/s	η, μm	τ, μs
2	0	1186	86.6	1080	133	10	0.7
	0.156	1184	64.6	1078	133	12	1.1
	0.369	1053	107	955	108	7	0.5
	0.44	675	196	847	89.1	4	0.2
	0.53	265	138	680	63.1	4	0.25
10	0	972	162	960	109	6	0.3
	0.3	767	236	864	92.0	4	0.2
	0.55	492	235	726	69.7	3	0.1
	1.05	186	135	488	35.6	3	0.2
	1.563	60.4	79.2	360	21.7	3	0.4
20	0	312	113	600	50.9	4	0.3
	0.365	300	114	590	49.4	4	0.3
	0.865	228	109	547	43.3	4	0.3
	1.365	157	93.9	489	35.7	3	0.3
	2.115	80.9	67.5	391	24.8	3	0.5
40	0	122	50.9	418	27.6	5	0.7
	0.5	121	50.9	420	27.8	5	0.7
	1.375	106	50.2	402	26.0	4	0.7
	3.25	60.7	42.4	364	22.1	4	0.9
	5.125	30.2	31.1	330	18.6	5	1.3

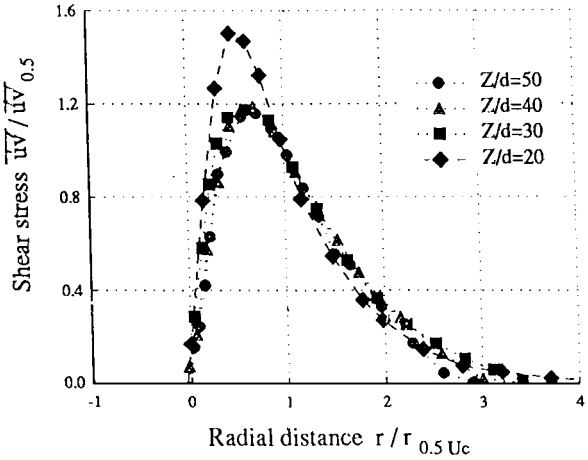

Fig. 10 Similarity of turbulence shear stress profiles for the coaxial jets.

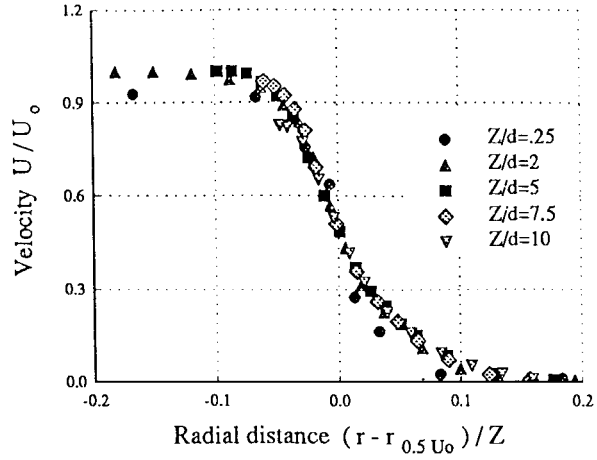

Fig. 11 Normalized mean axial velocity profiles for the single jet.

curve. However, the similarities of the turbulence quantities of the coaxial jets are observed at sections $Z/d = 30$–50 but not at section $Z/d = 20$ (Figs. 9 and 10). This indicates that developments of turbulence parameters are slower than that of the mean velocity; i.e., turbulence parameters need more time to reach local invariance. Similarities of the mean axial velocity, turbulence kinetic energy, and shear stress for the single jet at $Z/d \geq 15$ are observed. Comparing the velocity similarity with the temperature similarity suggests that the velocity self-similarity is established downstream of the temperature self-similarity. This is because the heat transfer is faster than the momentum transfer or the Prandtl number is less than 1.

The normalization of the mean axial velocity of the single jet at upstream sections ($Z/d \leq 10$) is shown in Fig. 11. The coordinates are U/U_0 and $\eta = (r - r_{0.5U_0})/Z$, where U_0 is the jet exit velocity. Except for the initial section at $Z/d = 0.25$ ($Z = 2$ mm), the mean axial velocity profiles at these upstream sections can be approximated by a universal distribution. For the upstream region of the coaxial jets, the flow pattern is complicated and strongly dependent on the geometry and exit condition of the flow, and no simple normalization form is available.

Fluid Turbulent Scales

In turbulent flows, a wide range of length scales exists, from the dimensions of the flowfield to the diffusive action of molecular viscosity. Kolmogoroff scales are considered as the smallest scales in turbulent flows. Following the estimation of Cheng et al.,[16] the Kolmogoroff length scales and timescales were calculated from the velocity and density measurements in the present work. Table 1 gives the axial mean velocity, fluctuating velocity $\sqrt{(\bar{u}'^2+\bar{v}'^2+\bar{w}'^2)}$, temperature, kinematic viscosity, Kolmogoroff length scale η, and timescales τ at various radial positions of four sections of the single jet. Table 1 indicates that the smallest turbulent scales are on the order of 5 μm and 0.5 μs, respectively. The estimated integral length scales, which are not shown in Table 1, are 2.6, 3.2, 7.6, and 18.2 mm for $Z/d = 2$, 10, 20, and 40, respectively; the corresponding ratios of the LDV control volume length to the integral length scale are 0.23, 0.19, 0.08, and 0.03. Goulard et al.[17] suggest that the spatial and temporal resolution of the experimental systems should be less than three times the Kolmogoroff scales. The time resolution of the LDV setup satisfies this requirement; however, the LDV spatial resolution does not meet this criterion. Recently, Mansour and Bilger[18] studied the effects of spatial averaging on Raman/Rayleigh measurements and pointed out that, if the probe length is 0.3 times the integral length scale, a measurement would capture at least 85% of the variance scalar for the turbulent Reynolds number range from 50 to 500 (based on the integral scale). Based on the estimation of Mansour and Bilger, we know that at least 80% of the variance scales in this flow will be captured with the present LDV setup.

General Flowfield Characteristics

The time-averaged velocity vector and streamline plots for sections $Z/d = 0.25$–20 of the coaxial jets are shown in Fig. 12. The upper half of the plot shows the velocity vectors, and the lower part illustrates the time-averaged streamlines. A recirculation region is

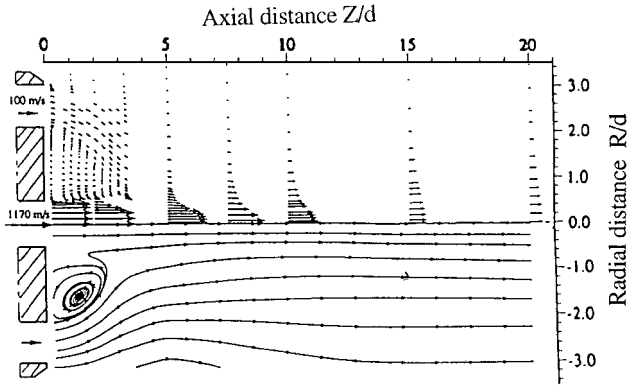

Fig. 12 Velocity vector and streamline plots of the coaxial jets, *Z/d* = 2–20.

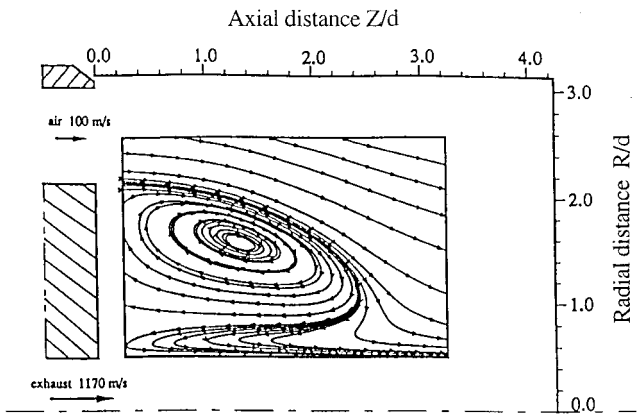

Fig. 13 Streamline plot of the recirculation region.

formed near the bluff base. The annular flow is forced toward the center axis by the central jet and impinges on the central jet between $Z/d = 3$ and 5, which agrees with the flow pattern shown in the schlieren photo. Because of the existence of the annular jet in the coaxial flow, the streamlines are more or less parallel downstream.

Like all base flows behind a bluff body,[19] the pressure in the recirculation region is lower than the surrounding flow due to the flow path's sudden expansion. The pressure in the recirculation region was assessed by a pitot tube and a precision vacuum gauge. The minimum pressure was 0.033 bar lower than the ambient pressure in the recirculation zone adjacent to the annular jet and 0.066 bar lower than the ambient pressure in the narrow recirculation zone adjacent to the central jet. This introduces a maximum error of 7% for the temperature inferred from the density measurement in this narrow region.

To gain more insight into the recirculation region of the coaxial flow, we mapped the recirculation region in detail with the LDV system. The streamline plot is shown in Fig. 13. It is interesting to note that one and a half recirculation zones, instead of two, are found. A portion of the annular flow moves around the envelope of the recirculation zone, hits the bluff-base surface, then turns another 180 deg (entrained by the central jet), and mixes with the central jet. The low pressure in the recirculation region created by the central and annular flows is not strong enough to force the central jet to reverse, and part of the reverse flow from the annular air is forced to follow the central high-velocity flow. The velocity field in the half recirculation zone was surveyed by the LDV with small step sizes (0.5 mm in the axial direction), and no negative mean axial velocity was found, which meant that the recirculation zone created by the central jet was not complete. To confirm the LDV experimental results, a fine thermocouple was employed to check the temperature in this region. The temperature in the recirculation region was only 25 K above the airflow temperature, which was close to that obtained with the Rayleigh scattering technique. Because the heat transfer between the central jet and recirculation region is very strong due to steep temperature gradients between them, the temperature of the flow in the recirculation region adjacent to the central jet is high. If a complete recirculation zone was formed adjacent to the central jet, the high-temperature fluid adjacent to the central jet would reverse its direction and return into the recirculation zone. Consequently, the temperature in the recirculation zone would be much higher than 25 K above the ambient temperature. However, due to the incompleteness of the recirculation zone adjacent to the central jet, the heat transfer between the central jet and base region depends only on radiation and turbulent mixing, not on convection by the reverse flow. As a result, the temperature in the recirculation region is only slightly higher than the ambient temperature.

Schefer et al.[19] pointed out that the flow structure of a coaxial flow with a bluff body is affected by the ratio of axial momentum between two jets and their geometry. They studied annular-jet-dominated combusting and noncombusting flows in great detail with two-dimensional LDV. Their central fuel jet velocity was 21 m/s with a nozzle exit diameter of 5.6 mm; the annular air velocity was 25 m/s, and the annular channel width was 25 mm with a bluff-body diameter of 50 mm. The axial momentum ratio of the central fuel jet to the annular air (at the exit) was only 1:650, and the kinetic energy ($\rho U^2/2$) ratio was 1:2.55. The central fuel–jet momentum was so weak that the central fuel jet could not penetrate the envelope of the annular recirculation region, and the central fuel flow was completely enclosed by the annular flow. In their case, two counter-rotating vortices were clearly defined. One was located adjacent to the upstream portion of the fuel jet and rotated in a counterclockwise direction, which was driven primarily by the central fuel jet. A second vortex, rotating in a clockwise direction, was located adjacent to the shear layer established along the annular airflow. The volumes of these two vortices were comparable.

With increasing central jet velocity, the central flow will penetrate the annular recirculation region and eventually dominate the flow structure. Pang[20] studied the turbulence structure of air/air coaxial jets separated by a bluff body, which had the same geometry as the present study. The central flow was 300 m/s, and the annular flow was 100 m/s. The axial momentum ratio between the central and annular jets was 1:2.1, and the kinetic energy ratio was 9:1. It was found that two counter-rotating recirculation zones were formed above the base. The inner vortex formed primarily by the central jet was much smaller than the vortex established primarily by the annular jet.

For the present coaxial jets, the velocity of the central jet is very high (~1200 m/s), and the velocity ratio between the central jet and annular jet is quite large (12/1). The axial momentum ratio of the central jet to the annular jet is 2:1, and the kinetic energy ratio is 37.6:1. In the time-averaged sense, no fluid from the central jet is reversed. This particular flow pattern represents an extreme operating condition of the central-jet-dominated coaxial flows.

Conclusions

The flowfields of a supersonic high-temperature exhaust plume with and without a base flow have been experimentally investigated. Comprehensive analyses and tests were carried out with a two-dimensional LDV system and a Rayleigh scattering system.

Mean velocity components, turbulence intensities, shear stress, turbulence kinetic energy, mean density, temperature, and Mach number are obtained for both the single jet and coaxial jets. The temperature profiles of the coaxial jets are similar to those of the single jet. The radial distributions of the mean temperature can be expressed in self-similar form $Z/d = 10$ downstream for both the single and coaxial jets. The potential core length for both flows extends about six nozzle diameters, which is verified by both velocity and temperature measurements. Both flows remain supersonic until $Z/d = 14.5$. The radial distributions of the mean axial velocity, turbulence kinetic energy, and shear stress can be expressed in self-similar forms at downstream regions for both the single jet ($Z/d \geq 15$) and the coaxial jets ($Z/d \geq 30$) The establishment of similarity of mean velocity is upstream of the turbulence quantities, and the temperature field reaches self-similarity sooner than the velocity field. Because of the enhancement of turbulent mixing by the flow recirculation and the impingement between the central jet and annular jet, the decay of the mean axial velocity, temperature, and Mach number in the coaxial jets is faster than that in the single jet at the upstream sections jet ($Z/d \leq 10$).

Detailed LDV measurements of the recirculation region in the coaxial flow reveal that only one and a half, instead of two, recirculation zones are formed above the bluff base. It represents an extreme case of the central-jet-dominated coaxial flows.

References

[1]Lau, J. C., Morris, P. J., and Fisher, M. J., "Measurements in Subsonic and Supersonic Free Jets Using a Laser Velocimeter," *Journal of Fluid Mechanics*, Vol. 93, Pt. 1, 1979, pp. 1–27.

[2]Lau, J. C., "Effects of Exit Mach Number and Temperature on Mean-Flow and Turbulence Characteristics in Round Jets," *Journal of Fluid Mechanics*, Vol. 105, 1981, pp. 193–218.

[3]Dimotakis, P. E., "Turbulent Free Shear Layer Mixing and Combustion," *High Speed Flight Propulsion Systems*, edited by S. N. B. Murthy and E. T. Curran, Vol. 137, Progress in Astronautics and Aeronautics, AIAA, Washington, DC, 1991, pp. 265–340.

[4]Petrie, H., and Walker, B. J., "Comparison of Experiment and Computation for a Missile Base Region Flowfield with a Centered Propulsive Jet," AIAA Paper 85-1618, July 1985.

[5]de Groot, W. A., and Weiss, J. M., "Species and Temperature Measurement in H_2/O_2 Rocket Flow Fields by Means of Raman Scattering Diagnostics," AIAA Paper 92-3353, July 1992.

[6]Cheng, T. S., Wehrmeyer, J. A., Pitz, R. W., Jarrett, O., Jr., and Northam, G. B., "Raman Measurement of Mixing and Finite-Rate Chemistry in a Supersonic Hydrogen-Air Diffusion Flame," *Combustion and Flame*, Vol. 99, No. 1, 1994, pp. 157–173.

[7]Jiang, L.-Y., and Sislian, J. P., "LDV Measurements of Mean Velocity Components and Turbulence Intensities in Supersonic High-Temperature Exhaust Plumes," AIAA Paper 93-3069, July 1993.

[8]Jiang, L. Y., and Sislian, J. P., "Turbulent Mixing in Supersonic High-Temperature Exhaust Jets," Inst. for Aerospace Studies, Univ. of Toronto, Rept. 351, Downsview, ON, Canada, Feb. 1996.

[9]Owen, F. K., and Calarese, W., "Turbulence Measurement in Hypersonic Flow," Aerodynamics of Hypersonic Lifting Vehicles, AGARD Conf. Proceedings No. 428, Paper No. 5, April 1987.

[10]Boutier, A., Lefevre, J., and Micheli, F., "Laser Velocimetry for Hypersonic Flows," 4th International Conf. on Laser Anemometry, Cleveland, OH, Vol. 2, 1991, pp. 457–463.

[11]Eckbreth, A. C., *Laser Diagnostics for Combustion Temperature and Species*, Abacus, Cambridge, MA, 1988.

[12]Long, M. B., "Multidimensional Imaging in Combusting Flows by Lorenz–Mie, Rayleigh, and Raman Scattering," *Instrumentation for Flows with Combustion*, edited by A. M. K. P. Taylor, Academic, London, 1993, pp. 467–508.

[13]Dibble, R. W., and Hollenbach, R. E., "Laser Rayleigh Thermometry in Turbulent Flames," *18th Symposium (International) on Combustion* (Waterloo, ON, Canada), Combustion Inst. Pittsburgh, PA, 1981, pp. 1489–1499.

[14]Otugen, M. V., and Namer, I., "Rayleigh Scattering Temperature Measurements in a Plane Turbulent Air Jet at Moderate Reynolds Numbers," *Experiments in Fluids*, Vol. 6, No. 7, 1988, pp. 461–466.

[15]von Glahn, U. H., "On Some Flow Characteristics of Conventional and Exited Jets," AIAA Paper 84-0532, Jan. 1984.

[16]Cheng, T. S., Wehrmeyer, J. A., and Pitz, R. W., "Simultaneous Temperature and Multispecies Measurement in a Lifted Hydrogen Diffusion Flame," *Combustion and Flame*, Vol. 91, Nos. 3, 4, 1992, pp. 323–345.

[17]Goulard, R., Mellor, A. M., and Bilger, R. W., "Combustion Measurements in Air Breathing Propulsion Engines. Survey and Research Needs," *Combustion Science and Technology*, Vol. 14, Nos. 4–6, 1976, pp. 195–219.

[18]Mansour, M. S., and Bilger, R. W., "Spatial-Averaging Effects in Raman/Rayleigh Measurements in a Turbulent Flame," *Combustion and Flame*, Vol. 82, Nos. 3, 4, 1990, pp. 411–425.

[19]Schefer, R. W., Namazian, N., and Kelly, J., "Velocity Measurements in a Turbulent Nonpremixed Bluff-Body Stabilized Flame," *Combustion Science and Technology*, Vol. 56, Nos. 4–6, 1987, pp. 101–138.

[20]Pang, C. K. W., "An Investigation of the Turbulence Structure of Isothermal High-Reynolds-Number Coaxial Air Jets with and Without a Bluff-Body," M.A.Sc. Thesis, Inst. for Aerospace Studies, Univ. of Toronto, Downsview, ON, Canada, 1991.

K. Kailasanath
Associate Editor